KARIRI SCIENCE
CECAPE Biology and Health Journal
v.2 n.1(2024): 7.
https://doi.org/10.29327/2256856.2.1-7
ISSN 2965-4084

https://faculdadececape.edu.br/revista-kariri-science/
CECAPE College
Juazeiro do Norte – CE – Brazil

Research Article

Influence of Abutment Height Behavior on Stress Distribution in TiO_2 Single Abutment: In vitro and Silico Validation

Jefferson D M de Matos [1,2,3]; Inácio J S Júnior [3]; Mário A C Sinhoreti [4]; Daher A Queiroz [5]; Jonas I Júnior [3]; Sidney L da Silva [6]; Rafael A da Silva [6]; Adriano B Barbosa [7]; Eric Padovani [7]; Jonas U R Schindler [7]; Nathália de C Ramos [1,9,10]; Cesar R Sakakura [11]; Marco A Bottino [1]; Milton Santamaria-Jr [3,8]; Alexandre L S Borges [1]; Guilherme da R S Lopes [1].

[1] Department of Biomaterials, Dental Materials, and Prosthodontics, Institute of Science and Technology, São Paulo State University (Unesp), São José dos Campos 05508-070, SP, Brazil; jefferson.matos@unesp.br (J.D.M.d.M.); nathalia.ramos@unesp.br (N.C.R.R.); marco.bottino@unesp.br (M.A.B.); guilherme.scalzer@unesp.br (G.d.R.S.L.); alexandre.borges@unesp.br (A.L.S.B.);
[2] Center for Dental Biomaterials, Department of Restorative Dental Sciences, University of Florida (UF Health), Gainesville, FL 32611, USA; melodematos.j@ufl.edu (J.D.M.d.M); sinhoreti@fop.unicamp.br (M.A.C.S.); MRocha@dental.ufl.edu (M.G.R.);
[3] Department of Dentistry, College of Dentistry CECAPE, Juazeiro do Norte 63024-015, CE, Brazil; inácio.junior@faculdadececape.edu.br (I.J.S.J.); jefferson.matos@unesp.br (J.D.M.d.M.); jonas.junior@faculdadececape.edu.br (J.I.J.);
[4] Department of Restorative Dentistry, Dental Materials Division, Piracicaba Dental School (FOP-UNICAMP), Piracicaba 13416-000, SP, Brazil; sinhoreti@fop.unicamp.br (M.A.C.S.);
[5] The University of Texas Health Science Center, Department of Restorative Dentistry & Prosthodontics, Houston (UTHealth) School of Dentistry, Houston 77054, TX, USA; daher.antonio.queiroz@uth.tmc.edu (D.A.Q.);
[6] Optical Group and Applications, College of Technology of Itaquera (FATEC), São Paulo 08295-005, SP, Brazil; sidney.silva6@fatec.sp.gov.br (S.L.d.S); rafael-alves1999@hotmail.com (R.A.d.S);
[7] Midwest Dental Arts Inc., Palm Bay, FL 32909, USA; adrianobaldotto@hotmail.com (A.B.B.); ericpadovani77@gmail.com (E.P.); jonasrschindler@gmail.com (J.U.R.);
[8] Deparment of Orthodontics, Centro Universitário da Fundação Hermínio Ometto (FHO), Araras 13607-339, SP, Brazil; santamariajr@fho.edu.br (M.S.J.);
[9] Department of Dentistry, Universidade São Francisco (USF), Bragança Paulista, SP, Brazil; nathalia.carvalhoramos@gmail.com (N.C.R.R.);
[10] Postgraduate Program in Dentistry, Department Dentistry, University of Taubaté (UNITAU), Taubate 12080-000, SP, Brazil; nathalia.carvalhoramos@gmail.com (N.C.R.R.);
[11] Laboratório CRS Proteses, Campinas 13070282, SP, Brazil; cesarsakakura@hotmail.com (C.R.S.);

***Correspondence:** jefferson.matos@unesp.br

Citation: Matos *et al.*, Influence of Abutment Height Behavior on Stress Distribution in TiO_2 Single Abutment: In vitro and Silico Validation

Kariri Science v.2 n.1(2024): 7. https://doi.org/10.29327/2256856.2.1-7

Associate Editor: Edinardo F.F. Matias

Received: 17 February 2024
Accepted: 10 July 2024
Published: 10 August 2024

Abstract: To evaluate the influence of universal abutment height on the biomechanical behavior and stress distribution of TiO2 single abutment. Six specimens with implants (4 × 10 mm) morse taper (Titaniumfix, São José dos Campos, SP, Brazil) made of commercially pure titanium were used. Three implants received the Short Universal Link (4.5 × 4 mm) (SUL) and three implants received the Long Universal Link (4.5 × 5.5 mm) (LUL). The two groups had their specimens investigated by different methodologies: strain gauge, digital image correlation, photoelasticity, and finite element method (FEA). After in vitro analyses, three-dimensional models of the two groups were created simulating all implant-supported restoration structures for computational analysis (FEA). Then, an oblique load of 100 and 200 N was applied on the central surface of the abutment of the evaluated groups (SUL and LUL). The analysis criteria were: the Von-Mises tension for the prosthetic components, bone microstrain, and total displacement. Stress maps were plotted on colorimetric graphs and maximum values were plotted on bar graphs. The distance between the abutment top and the implant/analog base was measured. To verify the clinical reproducibility of the experiment, comparisons were made between the height of the abutment for both groups evaluated (SUL and LUL), thus showing a greater discrepancy for the

LUL group ($p < 0.05$). To verify if the change in the test protocol could minimize the differences in the height of the prosthetic abutments, the abutment height of both groups was compared with two other validation tests of digital image correlation (DIC) and photoelasticity, with no significant difference being observed ($p > 0.05$). The data indicated that long collar abutments can negatively affect the biomechanical behavior of single structures supported by morse taper implants, and the greatest stresses are located in the prosthetic abutment. Therefore, long abutments directly influence the total length of the prosthetic abutments of morse taper implants.

Keywords: Dental Abutments; Dental Implants; Dental Materials; Bioengineering

1. Introduction

The success of implant-supported single-unit rehabilitation does not depend only on osseointegration, but on the stability of peri-implant tissues, as it plays a fundamental role in function and aesthetics. The magnitude of the masticatory load influences, both qualitatively and quantitatively, the biomechanical performance of osseointegrated implants and, consequently, the success of these rehabilitations in the long term. [1,2]

The resultant masticatory loads on implant-supported rehabilitations may generate occlusal overload, which is considered one of the main factors in mechanical and biological failures. [3] In this sense, these loads may cause strain of the peri-implant bone beyond its physiological limit, biological failure, and even stresses that exceed the resistance of the restorative materials, with a consequent mechanical failure. [4]

Single-unit rehabilitations on implants allow the use of several components with different retention systems. However, the versatility of CAD/CAM abutments and their technological advantages have been part of the prosthetic solution of many companies, since these abutments have brought the advantages of cemented prostheses, by filling the space between the crown and the abutment, in addition, to allow access to the fixation screw, which guarantees the reversibility of the restorative system. [5] This technology allows a prosthetic design with the presence of a ceramic mesostructure between the abutment and crown and even cementation of the ceramic crown directly on the abutment, both options being good restorative alternatives. [6,7]

It is essential to understand how masticatory loads will influence the biomechanical behavior of rehabilitation with osseointegrated implants, since similar prosthetic abutments may present different behavior for the same load. [8] Even with the availability of CAD/CAM abutments with different heights among different implant companies, there are still no studies on peripheral stresses and strain, that is, little information is available regarding the influence of this magnitude on the biomechanical behavior of these restorations. [9]

Thus, we have that laboratory analyzes may provide qualitative and quantitative information on the pattern of tension transfer and facilitate the understanding of some clinical manifestations. [10,11] When different methodologies are used in the same investigation, they allow an analysis with fewer biases, in addition to allowing the use of a validated theoretical model, that is, a more precise computational analysis. [11,12]

Therefore, the present study aimed to evaluate the influence of universal abutments with different heights on the biomechanical behavior and stress distribution of titanium single abutments, through the main bioengineering tools, among them, finite element analysis, photoelastic, strain gauge, and digital correlation image.

2. Materials and Methods

Six implants (4 x 10 mm) of morse taper (Titaniumfix, São José dos Campos, SP, Brazil) made of commercially pure titanium were used. Three implants received the 4.5 x 4 mm Short Universal Link (SUL) and three implants received the 4.5 × 5.5 mm Long

Universal Link (LUL). These pillars feature a 6° conical design and internal friction fit. The abutments were installed with a torque of 35 N.cm, using a specific wrench from the Titaniumfix System (Complete Prosthetic Kit, São José dos Campos, SP, Brazil). Torques were confirmed 10 min after installation, before, and at the end of the strain gauge test. The specimens were made using PVC tubes with a diameter of ¾ inch, where the implants were stabilized by a polyurethane resin (F160, Axson Technologies, Saint-Ouen-I`Aumône, France). 3 mm of the implants will remain exposed above the resin simulating an unfavorable clinical condition as per ISO for fatigue of dental implants ISO 14801:2017. [13] The tests were performed by a single trained operator and the samples were randomly numbered before the tests and were performed within their groups.

2.1. Finite Element Analysis (FEA)

Using CAD software (Rhinoceros 5.0, McNeel Europe™, Barcelona, Spain), all structures were modeled according to the specifications and geometry of each material and the set gave rise to the final model for each group.[14] Thus, a three-dimensional (3D) structure was modeled to represent a parallelepiped-shaped section (20 × 40 mm), containing polyurethane (95 × 45 × 30 mm) and photoelastic resin. [15] Based on the therapeutic possibilities for the same clinical indication, a single system was formed. However, a slight difference could be noticed in the height of the column. [14,16] The models were distributed in the respective study groups: SUL (control): Short Universal Link (T-base Abutment 4.5 × 4 mm, Bone Level, Titaniumfix, São José dos Campos, SP, Brazil) and LUL (experimental): Long Universal Link (4.5 × 5.5 mm T-base Abutment, Titaniumfix, São José dos Campos, SP, Brazil). Then, the specimen section model was submitted to an implant (Blackfix Profile Implant - 4 × 10 mm, Bone Level, Titaniumfix, São José dos Campos, SP, Brazil) according to the system of each group. To simulate a condition closer to the clinical practice already reported in the literature, [15] the entire implant and abutment set were positioned on the base as shown in Figure 1.

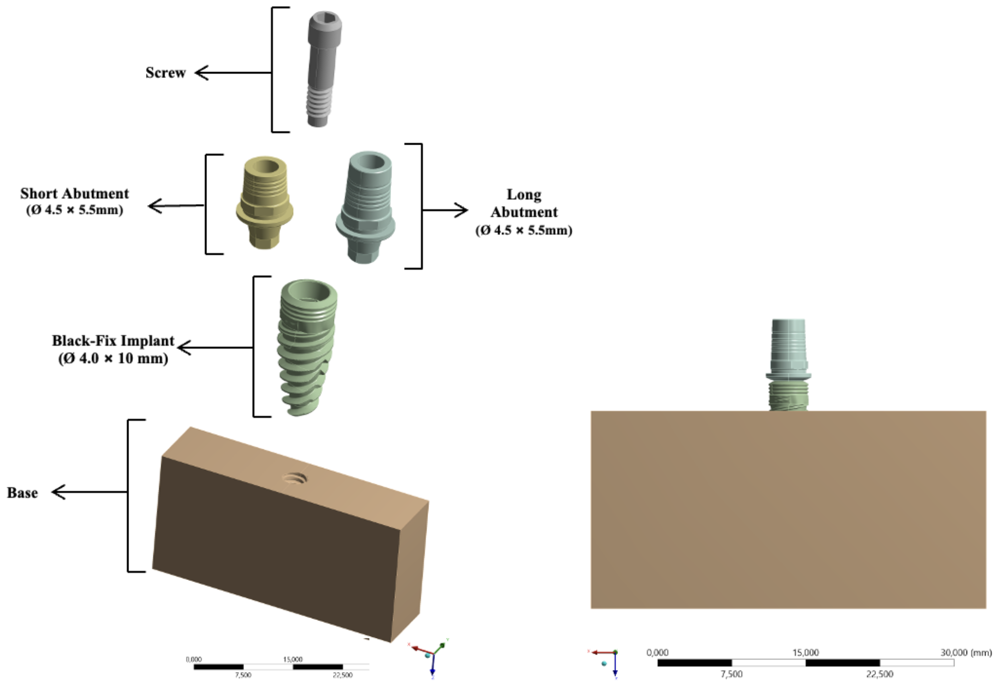

Figure 1. Illustrative of 3D models following the clinical sequence of an implant-supported prosthesis using the short abutment and large abutment implant systems.

Then, the solids were exported in STEP (STandard for the Exchange of Product model data) format for software analysis (ANSYS 17.2, ANSYS Inc., Houston, TX, USA).

The outer surface of the specimen section was fixed in all directions, applying an oblique load of 100 and 200 N to the central surface of the prosthetic abutment, specifically at the entrance of the prosthetic screw. A mesh was created after the 10% convergence test [14,16] corresponding to 952,108 nodes and 709,276 tetrahedral elements for the evaluated models (Figure 2). All materials were considered isotropic, linear, elastic, and homogeneous. Between the implant and the bone, the contact was used to simulate complete osseointegration [16], and the other contacts were considered glued.

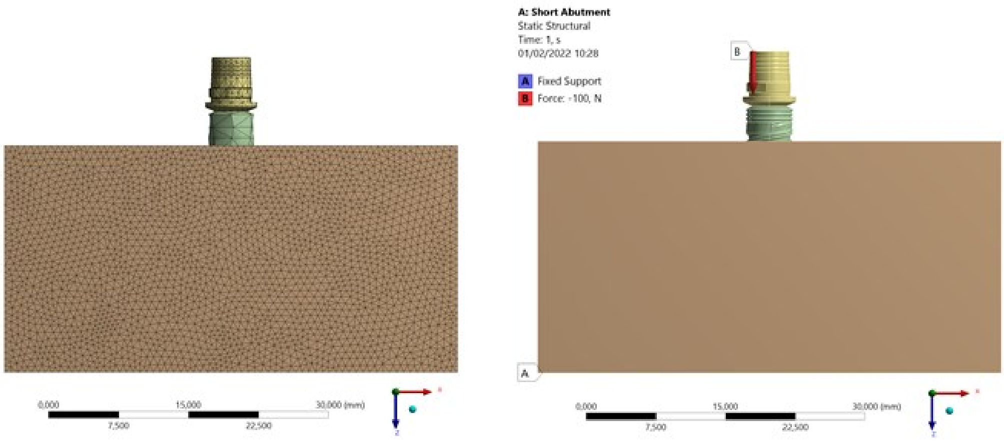

Figure 2. FEA details - Mesh, boundary conditions, loads, and connections.

The physical properties of the 3D model structures were defined based on the literature (Table 1). According to the Von-Mises criteria, the stress distribution results were exhibited using visual plots with a scale in megapascals (MPa) for implants and structures. The microstrain criteria were used to investigate the bone behavior and its maximum values are shown in Table 2 [17,18].

Table 1. Properties of the material used in the study.

Material	Composition	Young Modulus (GPa)	Poisson ratio
Titanium [18]	Titanium alloy ASTM F136	110	0.30
3-YTZP [19]	8 mol% Y-TZP: ZrO_2 principal component, Y2O3< 12 %, Al2O3< 1 %, SiO2<0.02 %, Fe2O3 < 0.02 %	220	0.30
Resin Cement [20]	10-MDP, hydrophobic aromatic and aliphatic photoinitiator, dibenzoyl peroxide dimethacrylate, hydrophilic dimethacrylate, silanized silica	7.5	0.25
Polyurethane [21]	Poly[oxy(methyl-1,2-ethanediyl)], .alpha.-hydro-.omega.-hydroxy-, polymer with 1,1'-methylenebis[4-isocyanatobenzene] 4,4'-Diphenylmethane diisocyanate Benzene, 1,1'-methylenebis[4-isocyanato-, homopolymer] 4-methyl-1,3-dioxolan-2-one	3.6	0.30

Photoelastic Resin [22]	Bisphenol A and F Epoxy Resin + Aliphatic Glycidyl Ether + Epichlorohydrin = GDRFA	2.07	0.41

Stress and strain results that present values with a difference of less than 10% may be located in the convergence range of the analysis software, making it impossible to assume a significant difference. Consequently, the results presented that a difference in peak values greater than 10% will be considered significant. The results of each structure of both groups were compared qualitatively and quantitatively. Microstrain, von-Mises stress, and Maximum Principal Stress were adopted as failure criteria.

2.2. Strain gauge analysis

The methodology of linear strain gauge was used to validate the mathematical model and correlation of cervical bone strain. Therefore, one specimen from each group was randomly selected for the strain gauge analysis. That said received a linear strain gauge in the buccal, lingual, mesial, and distal polyurethane regions. polyurethane blocks (95 x 45 x 30 mm) (Polyurethane F16 Axson, Cercy, France) were manufactured to simulate an isotropic substrate for each group. The polyurethane resin polymerization was carried out to prevent pores in a vacuum pressurizer (Protecni, Araraquara, São Paulo, Brazil). After the polymerization, the blocks were removed from the matrix and their surfaces were polished with progressive sandpaper (#220 to #600 grit) underwater. Thus, the surfaces of the specimens were cleaned with isopropyl alcohol and an electric linear strain gauge model KFG-02-120-C1-11 (Kyowa Electronic Instruments Co., Ltd –Tokyo– Japan) was bonded to each cylinder with a cyanoacrylate-based adhesive (Super Bonder Loctite, São Paulo – Brazil), positioned on the region of highest stress concentration calculated by the FEA.

A metallic die [14] was used to standardize the implant placements (Blackfix Profile Implant - 4 × 10 mm, Bone Level, Titaniumfix, São José dos Campos, SP, Brazil), perpendicular to the surface, 3mm above bone level to simulate an unfavorable condition. [13] The respective abutments SUL (control): Short Universal Link (T-base Abutment 4.5 × 4 mm, Bone Level, Titaniumfix, São José dos Campos, SP, Brazil) and LUL (experimental): Long Universal Link (4.5 × 5.5 mm T-base Abutment, Titaniumfix, São José dos Campos, SP, Brazil). They were installed with the aid of a manual torquemeter and a new measurement to confirm the torque was performed using a digital torquemeter. All t-base abutments were screwed into the implants with 20 N.cm, according to the manufacturer's recommendation, using a torque wrench (Titaniumfix, São José dos Campos, SP, Brazil).

The surface of the blocks was cleaned with isopropyl alcohol and four unidirectional linear SGs model PA-06-060BA-120-L (Excel Sensores Ind. Com. Exp. Ltda, Taboão da Serra, São Paulo, Brazil, resistance 120 Ω; gauge length: 1.5 x 1.3 mm) were bonded to the surface of each block with cyanoacrylate adhesive (Super Bonder Loctite, São Paulo, Brazil). SG1 was placed mesially adjacent to implant #11, SG2 and SG3 were placed mesially and distally adjacent to implant #11 and SG4 was placed distally adjacent to implant #11 [15].

Each strain gauge was measured using a multimeter device (Minida ET 2055: Minida São Paulo - Brazil). The electrical resistance variations were transformed into a microstrain unit using an electrical signal conditioning device (Model 5100B Scanner – System 5000 – Instruments Division Measurements Group, Inc. Raleigh, North Carolina – USA). Data recording was performed using strain-smart software. Electrical cables allowed the connection between the strain gauges and the data acquisition device. Then, an axial load of 100 and 200 N was applied to the central surface of the prosthetic abutment. Data were generated in microstrain values.

Each strain gauge outlet was measured using a multimeter (Minida ET 2055: Minida São Paulo, Brazil), ensuring that the connector output had the same resistance (120 Ω)

[18]. Four electrical cables were installed at the outputs and connected to an electrical signal conditioning apparatus (Model 5100B Scanner – System 5000 – Instruments Division Measurements Group, Inc. Raleigh, Carolina do Norte – USA, FAPESP proc: 07/53293-4) to record variations in electrical resistance and convert them in microstrain ($\mu\varepsilon/\mu\varepsilon$).

2.3. Photoelastic Analysis (PA)

An implant with a diameter of (4 × 10 mm) was selected and inserted according to the recommendations of ISO 14801:2007. Thus, being exposed 3 mm above the resin simulates an unfavorable clinical condition according to the ISO for fatigue of dental implants (ISO 14801:2007). This preparation has been extensively considered in an attempt to simulate an unfavorable clinical condition, as mentioned above.

The implant samples were placed in a photoelastic resin following the manufacturer's instructions. Epoxy resin (Araldite®, TekBond, Saint Gobain, Embu das Artes, São Paulo, Brazil) and an epoxy resin hardener (Aradur®, Huntsman Container Corporation, Salt Lake City, UT, USA) were mixed (2:1). [22] Next, the material was injected into the previously obtained mold. After that, the implants on the photoelastic resin were stored in a container box and kept at room temperature for 72 hours until complete polymerization of the resin.

After resin polymerization, the implants were removed from the molds and stored at 37°C for 24 hours to allow the release of residual stresses that could be present in the photoelastic resin. Before fitting the prosthetic abutments, the implants on the photoelastic resin were positioned between the polarizing filters to determine if there was tension due to the fabrication or handling of the specimen; if so, the specimens were stored again until the stress was completely released. Each specimen on the photoelastic resin received an implant-supported restoration. The restoration was cleaned in an ultrasonic bath (Elma ultrasonic E15H, Singen, Germany) with distilled water for 15 s and dried with compressed air for 30 s. After completion of the cleaning steps, each sample was placed between two flat polarizing filters over white light forming a 90° angle to obtain a constant light field. The images obtained with the polariscope were captured by a professional digital camera. Based on the "Optical-Stress Law", the stress generated by the polymerization shrinkage of the composite resin was qualitatively analyzed from the photoelastic fringes that formed in the photoelastic resin, and the samples were compared after setting and 24 h. All samples were stored in a container at room temperature during the evaluation period.

2.4. Digital Image Correlation (DIC

The digital image correlation technique was performed to measure the strain generated on the surface of the photoelastic resin block for the different load applications. [23] A professional camera (Canon EOS Rebel T5 with Tamron 90 mm f/2.8 SP VC AF Macro-Lens) was used to capture the body strain images and a specialized software package (Gom correlate, Vtech Consulting Ltda, São Paulo, Brazil) was used for image analysis. The camera had a resolution of 18.00 megapixels. The surface of the resin model facing the camera lens was individualized with a thin layer of white spray. Then black spray was used to produce irregularly shaped spots for tracking analysis during image correlation. A non-impact progressive static load of 100 and 200 N was applied using a universal testing machine (DL-1000, EMIC, São José dos Campos, Brazil).

To measure the generated strain (mm) on the surface of the block, sequential images were obtained at a frequency of 1 Hz until the maximum load was reached. The first image was taken without loading, and the remaining images were compared with the first image to calculate surface displacements. The strain was calculated from displacement using image correlation software (GOM Correlate, Braunschweig, Germany). The cervical regions of both implants were selected to quantify the values [24-26].

3. Results

The results of a linear strain gauge, photoelasticity, and digital image correlation; were used to validate the mathematical model in the finite element analysis. Microstrain and Von-Misses stress (MPa) data were selected as failure criteria and qualitatively compared between the two groups.

3.1. Finite Element Analysis (FEA)

For a better analysis of the data, the values were transformed into modules and, according to the Shapiro-Wilk test, the results obtained showed a non-normal distribution ($p = 0.000$) (Table 2).

Table 2. Shapiro-Wilk normality test.

Process data	με (dp)
Stats: Shapiro-Wilk	0.860
p-value	0.019

The observation of the non-normal distribution by the Shapiro-Wilk test ($p < 0.05$), and non-parametric statistical tests were used, with independent analyzes of the factors "Group" and "Load". Therefore, the group factor was submitted to the Mann-Whitney test for presenting two variables (SUL and LUL). The "Load" factor was also analyzed using the Mann-Whitney test as it presents two variables (10.2 kgf and 20.4 kgf).

Therefore, according to the microstrains (με) of the evaluated groups, it was not possible to observe a statistical difference ($p = 0.720$) between the Long (119.1 ± 54.3 με) and Short (110.5 ± 49.7 με) (Table 3).

Table 3. Mann-Whitney test table for the "Group" factor for strain gauge.

Process data	με (dp)	W	p-value
SUL Group	119.1 ± 54.3	36	0.720
LUL Group	110.5 ± 49.7		

Analyzing the "Load" factor, the following means and standard deviations of microstrain (με) for the Loads of 10.2 kgf and 20.4 kgf were obtained: 98.5 ± 47.4 and 131.1 ± 51.0 με, respectively. With the statistical analysis, it was possible to observe that there was a statistical difference for this factor ($p = 0.037$) (Table 4).

Table 4. Mann-Whitney test table for the "Load" factor for strain gauge.

	με (dp)	W	p-value
10.2 kgf Load	98.5 ± 47.4	12	0.037
20.4 kgf Load	131.1 ± 51.0		

3.2. Digital Image Correlation (DIC)

For a better analysis of the data, the values were transformed into modules and, according to the Shapiro-Wilk test, the results obtained showed a non-normal distribution ($p = 0.000$) (Table 5).

Table 5. Shapiro-Wilk normality test.

Process data	με (dp)
Stats: Shapiro-Wilk	0.872
p-value	0.001

Because of the non-normal distribution by the Shapiro-Wilk test ($p<0.05$), non-parametric statistical tests were used, with independent analyzes of the factors "Group" and "Load". Therefore, the group factor was submitted to the Mann-Whitney test for presenting two variables (Long and Short). The "Load" factor was also analyzed using the Mann-Whitney test as it presents two variables (Load of 10.2 kgf and Load of 20.4 kgf).

Therefore, according to the voltages of the evaluated groups, it was not possible to observe a statistical difference ($p = 0.748$) between the LUL (1475.25 ± 1047.6 με) (Figure 3) and SUL (1090.7 ± 405.9 με) (Figure 4) groups (Table 6).

Table 6. Mann-Whitney test table for the "Group" factor for digital image correlation.

Process data	με (dp)	W	p-value
LUL	1475.25 ± 1047.6	137	0.748
SUL	1090.7 ± 405.9		

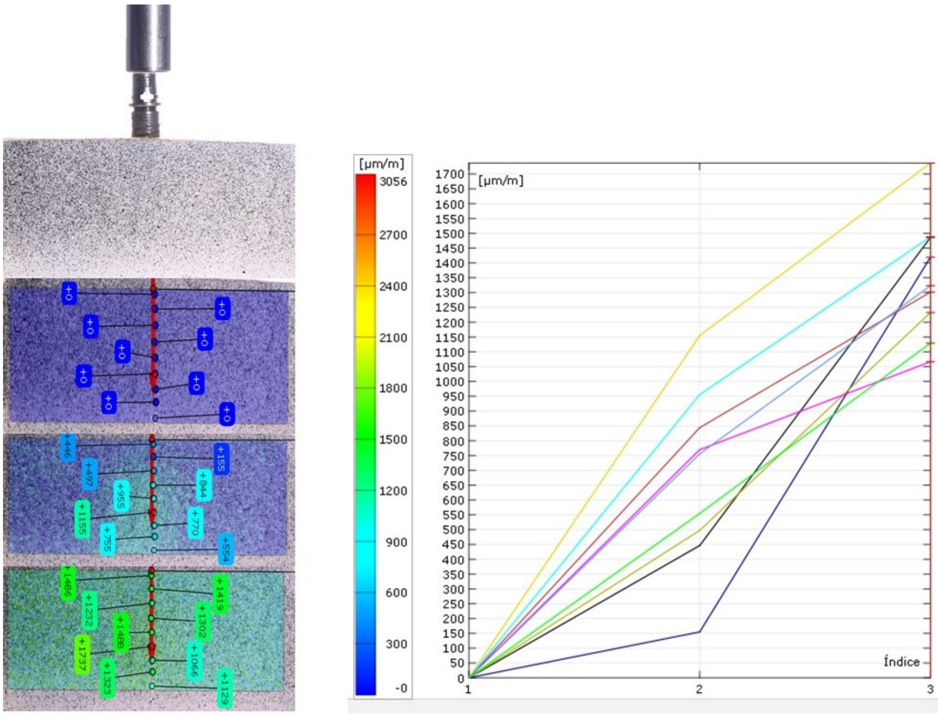

Figure 3. Digital image correlation analysis with the distribution of microstrain values (με) for the short column group.

Table 7. Mann-Whitney test table for the "Load" factor for digital image correlation.

Process data	με (dp)	W	p-value
10.2 kgf Load	609.8 ± 225.2	0	0.000
20.4 kgf Load	1956 ± 560.0		

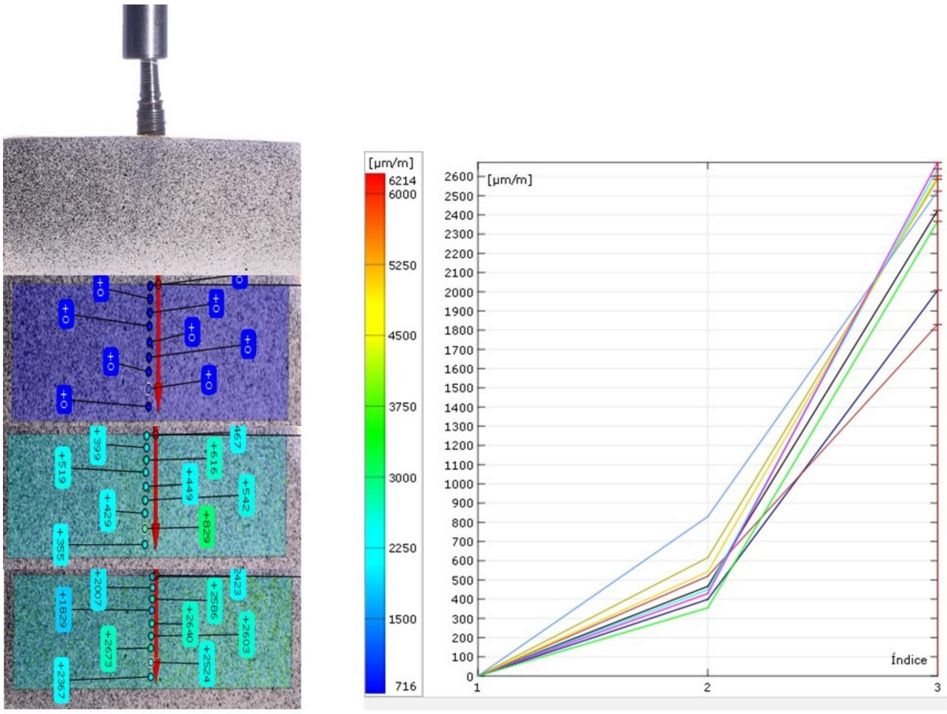

Figure 4. Digital image correlation analysis with the distribution of microstrain values (µε) in micrometers for the long-column group.

3.3. Finite Element Analysis (FEA)

In an extensive qualitative analysis, the displacement of the implant-abutment set can be verified in Figure 9. The mechanical responses were calculated according to the failure criteria of each structure. For bone tissue, the results were analyzed on strain based on previous studies. [26-28] Observing the strain distribution represented in Figure 9, it is possible to observe that there was a similar response pattern among the models for the strain generated in the cortical bone; however, the long abutment model has a greater magnitude of cervical tension than the short abutment model.

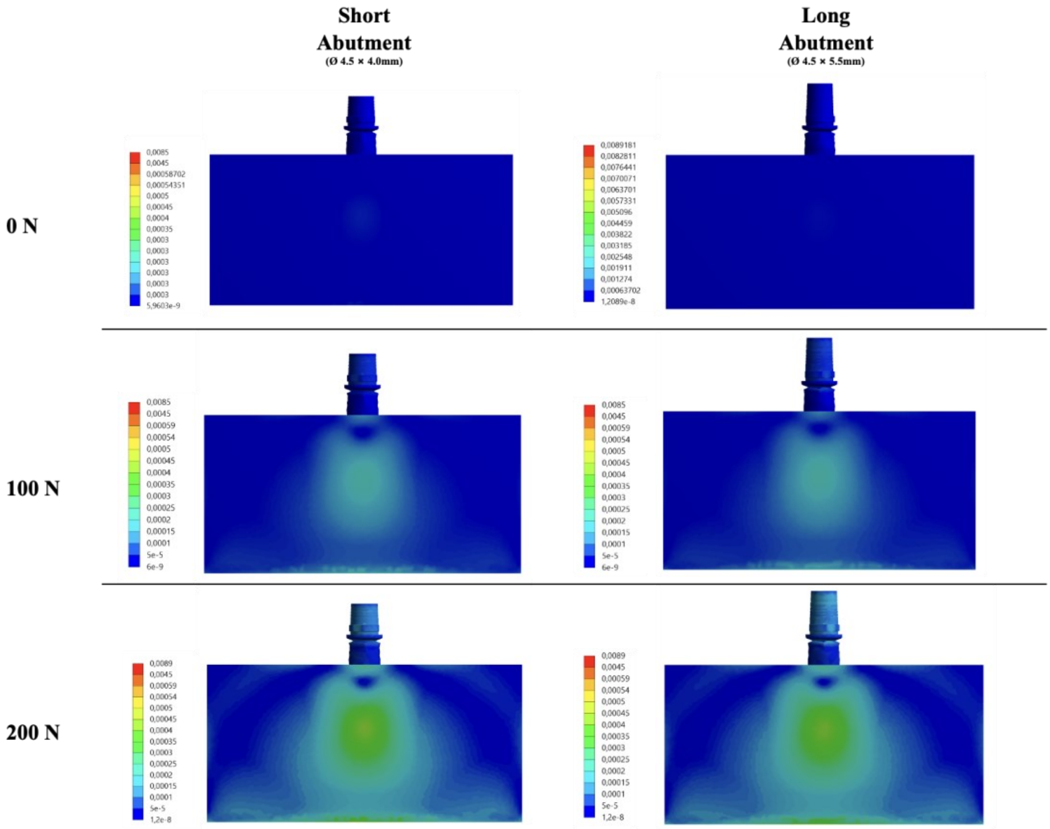

Figure 5. Illustrative of the 3D modeling qualitative analysis of Displacement and Strain Criteria on the structures of each group. A) Displacement Criteria. B) Strain Criteria. Left to Right: SUL: Short Universal Link (Control); LUL: Long Universal Link.

This behavior can be described by the strain and von-Mises stress map in Figure 10. In ductile solids, such as titanium implants and abutments, the stress results followed the von-Mises criteria that help to show the regions of onset of fracture in metals. However, for a comparative analysis between the models, the results generated were obtained by the von-Mises stress and also for the model with long pillars. The corresponding goes for the maximum principal stress, which highlights stress regions, the failure criterion for metals. Thus, both criteria present similar stress maps, but with different magnitude values, as plotted in Table 8. Thus, the long column concentrates more stresses in its structure, reducing the energy required for its displacement (Figures 5 and 6).

Table 8. Quantitative analysis of von-Mises stress results in stress peaks (MPa) in each group's structures and bone microstrains (με).

Analysis Criterion	**Group**	
	Long	**Short**
Displacement (mm)	00.42	00.56
Strain (μm/ μm)	00.0780	00.0798
Maximum Principal Stress (MPa)	280.76	250.11
von Mises stress (MPa)	266.69	278.39

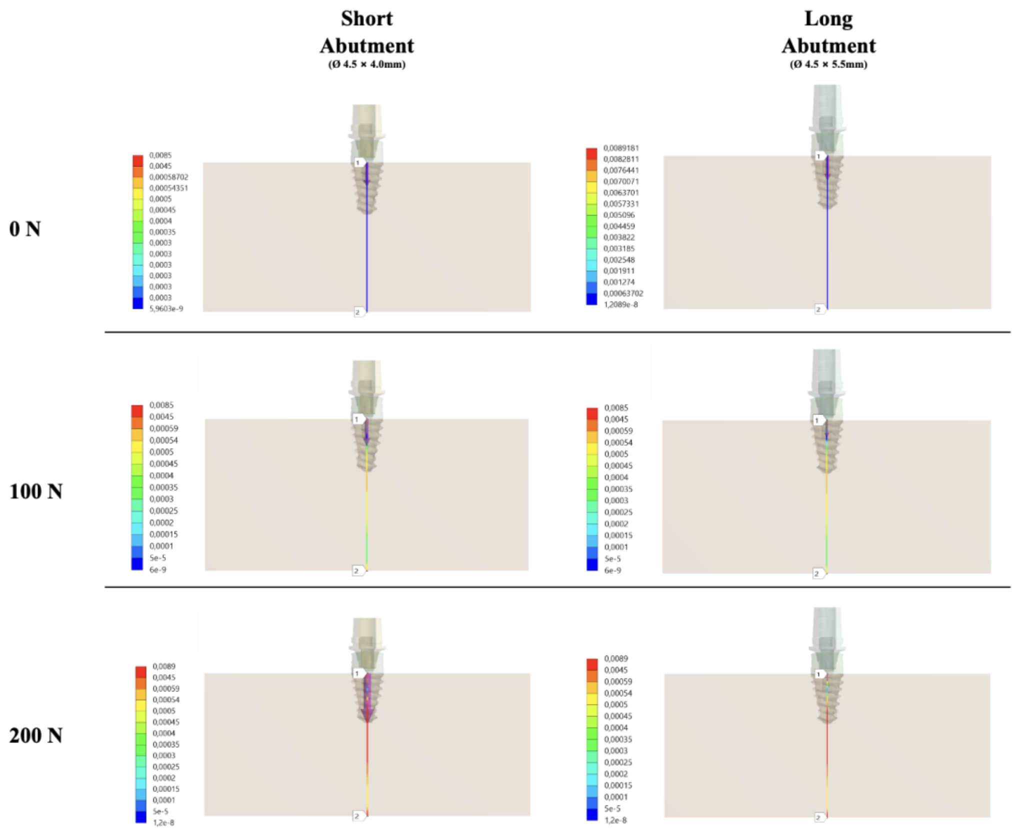

Figure 6. Illustrative of the 3D modeling qualitative analysis of Displacement and Strain Criteria on the structures of each group. A) Displacement Criteria. B) Strain Criteria. Left to Right: SUL: Short Universal Link (Control); LUL: Long Universal Link.

For a better analysis of the data, the values were transformed into modules and, according to the Shapiro-Wilk test, the results obtained showed a non-normal distribution ($p = 0.015$) (Table 9).

Table 9. Shapiro-Wilk normality test.

Process data	με (dp)
Stats: Shapiro-Wilk	0.915
p-value	0.015

The observation of the non-normal distribution by the Shapiro-Wilk test ($p < 0.05$), and non-parametric statistical tests were used, with independent analyzes of the factors “Group” and “Load”. Therefore, the group factor was submitted to the Mann-Whitney test for presenting two variables (Short and Long). The “Load” factor was also analyzed with the Mann-Whitney test as it presents two variables (Load of 100N and Load of 200N). Therefore, according to the microstrains of the evaluated groups, it was not possible to observe a statistical difference ($p = 0.692$) between the Short (186.5 ± 118.6 με) and Long (195.0 ± 121.3 με) groups (Table 10).

Table 10. Mann-Whitney test for the “Group” factor for FEA.

	με (dp)	W	p-value
LUL	186.5 ± 118.6	139	0.692

SUL	195.0 ± 121.3

Analyzing the "Load" factor, we have the following voltage averages and standard deviations for the 100N and 200N Loads: 127.5 ± 64.4 and 254.0 ± 127.0 με, respectively. With the statistical analysis, it was possible to observe that there was a statistical difference for this factor (p = 0.010) (Table 11).

Table 11. Mann-Whitney test for the "Load" factor for FEA.

Process data	με (dp)	W	p-value
100 N Load	127.5 ± 64.4	59.5	0.010
200 N Load	254.0 ± 127.0		

3.4. Photoelastic Analysis

The restored photoelastic models were analyzed using a transmission polariscope (Profile Projector Mitutoyo, Mitutoyo Corporation, Kawasaki, Japan). Images of the restored photoelastic models were recorded at the baseline (immediately), 15 min, 30 min, 60 min, 8 h, and 48 h after final polymerization. An extensive qualitative and quantitative analysis, obtained through a sequence of three thousand images resulting in a video obtained by the digital camera produced O = 8.5460 frames of images, of which were selected = 8.5447, divided into G = 12 groups of O/G = 420 image frames. The images were converted to the standard containing 256 shades of grey, 8-bit. [29]

The graph in Figure 8 shows the relationships between average external stresses versus average longitudinal strains for the photoelastic sample used. it was possible to observe the relative strain of the photoelastic resin, which involves the average area of the fringe length (Table 12). Mechanical responses were calculated according to the failure criteria of each structure. For bone tissue, the results were analyzed on strain based on previous studies. [26-28] Observing the relationship between the factors of mean external forces versus mean relative strain represented in Figure 7, it is possible to observe that there is a similar response pattern between the models for the strain generated in the cortical bone; however, the long abutment model has a greater magnitude of cervical tension than the short abutment model.

Table 12. Values for external force and average relative strain.

Process Data	εr (dr)
0 N Load / 0.0 kgf	1.1×10^{-3}
100 N Load / 10.2 kgf	5.5×10^{-3}
200 N Load / 20.4 kgf	11.1×10^{-3}

From the value tg (β) $\Xi < E >$= $(2.902 \pm 0.034) \times 10^{-2}$ GPa and the mean typical value of the mean optical dispersion coefficient obtained in the literature, Da Silva (2017) [30], $< C >$= $(2.79 \pm 0.13) \times 10^{-12}$m²/N, the mean dispersion factor was obtained, $< a_C >$ by stress equation, white your respective uncertainty, $\sigma(a_C)$, by strain equation, such that:

$$< a_C > = (8.90 \pm 0.42) \times 10{-}5,$$

$< a_C >$ is dimensionless, since the dimension of the modulus of elasticity, $[E]$, is the inverse of the dimension of the optical dispersion coefficient, $[C]$. [29, 30]

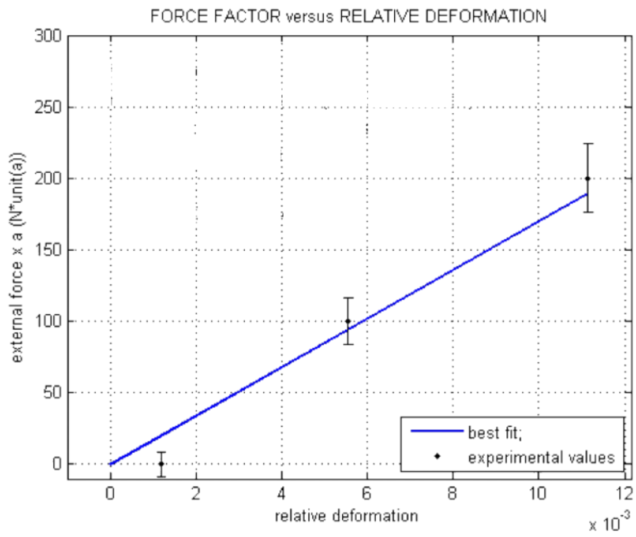

Figure 7. Linear regression graph of the force factor by the relative strain obtained by the computer system, from the algorithms.

Symmetrically moderate stress values were observed in both abutments alongside the applied force. In the group with the short abutment, the tension in the apical region was spread evenly throughout the entire restorative setup to the alveolar crest. In contrast, for the long group, fringes with moderate tension were observed on the apical side of the implant, and high tension in the coronal region of the bone crest of the ridge.

4. Discussion

The objective of this study was to evaluate the influence of universal abutment height on the biomechanical behavior and stress distribution of TiO2 single abutment on implants, through the main bioengineering tools, among them, finite element analysis, photoelasticity, strain gauge, and digital image correlation. The use of these bioengineering tools as a method to validate biomechanical behavior in vitro and silico has been widely used in dentistry, especially in implantology, to assess stresses and strains in dental implants and adjacent structures.[30] However, so far there is a lack of information in the literature regarding the use of the four methodologies, complementing and validating each other.

Interestingly, the von Mises stress values were used to assess the stresses observed along the implants under load. von Mises stress values are defined as the combined effect of the three main stress components, resulting in a single value, which is indicative of the beginning of stress distribution for ductile materials.[31] For implants, the maximum principal stresses were also adopted as a failure criterion, as failures occur when the stress is greater than or equal to the final strength of the material. [31.32]

The evaluation of the difference in biomechanical behavior between long and short abutments in implant-supported prosthesis cases preceded possible clinical studies. Therefore, this study evaluated the behavior of implants with different arrangements in the cobblestone region using computational models, as it allows the investigation of regions that are difficult to access by laboratory or clinical methods. [33-35] Admitting the fragility of titanium implants, it was considered more appropriate to use non-bonded implants with autonomous fixation systems. For this reason, the base designs allowed rotation of the prosthetic component during axial loading and transmission of the torsional load to the components and implant in the axial direction. [36,37] In this sense, allowing the prevention of overloads on the implant, since this function results in a greater transmission of force transferred to the marginal bone crest. [36-38]. It is interesting to clarify that the models were assumed to be homogeneous, isotropic, and linearly elastic.

The results obtained indicated that the abutment was the most damaged part of the implant during restoration, mainly for a high implant-to-abutment ratio of 1956 $\mu\varepsilon$. Tension increased by about 180% when a taller abutment (5.5 mm) was associated with a 10 mm implant. These results corroborate those of Machado et al. [39], who observed the predominance of abutment failure in vitro for morse taper implants that can be attributed to the large contact area between implants and abutments. The reliability of the assembly is challenged by the thick wall of the abutments in the collar region bent to the implant platform during axial loading [39,40]. Furthermore, a recent systematic review [41] proposed that an abutment-to-implant ratio greater than 1.46 may be related to prosthetic failure and pose a risk of abutment fracture. Regarding the prosthetic screws, there was a negative compromise in the implant and abutment set, with an increase in tension of up to 40%, regardless of the implant length.

Knowing that screw loosening is considered the most important reason for prosthetic failure during rehabilitation, especially for morse taper connections [39,40,42,43]. These prosthetic screw failures are more associated with two-piece abutments than with solid abutments, as they are thicker screws with less material that can dissipate load strain stress during mastication. A systematic review by Gracis et al. [44] pointed out interesting clinical results that can be analyzed during abutment selection to assess its failure potential: the fracture incidence of metal and zirconia abutments and abutment screws does not seem to be influenced by the type of connection; loosening of the abutment screws was still the most frequent technical complication, seeming to be directly influenced by the type of connection; and adequate preload can decrease the incidence of such a complication.

The relationship between occlusal forces on oral implants and the surrounding bone can be compromised by overload resulting in biological complications or even failure of osseointegration [45] or bone apposition. On the other hand, microdamage resulting from axial loading, followed by bone resorption, was soon followed by mechanical stress beyond the physiological limit [3]. The highest cortical microstrain stresses of 280.76 MPa were observed in the long pillar models. On the other hand, the short column group is 14% lower than the corresponding stresses in the 4.5 mm models. The region with the maximum principal stress was restricted to the peri-implant bone around the first implant threads. This corroborates the results of Rieger et al. [46], who demonstrated that high levels of tension induced during flexion are concentrated around the neck and are dissipated by the apex and throughout the cortical bone.

Recent studies suggest that the diameter of the implant should be more important than the length of the implants to control bone overload, since wide implants have greater bone-implant contact, especially in the cervical region, the tension is concentrated close to the threads of the first implant in contact with cortical bone [47, 48, 53]. The bone tensions obtained in this study were below the physiological limits described in the literature for the elastic limit of human cortical bone (60 MPa) [49]. However, the correlation between the bone's adaptive ability to distribute stress without biological damage is still unclear [50], since experimental studies have shown different biomechanical behaviors when oblique forces are involved leading to an increase in bone response [39, 41, 49].

Although a recent study [51] suggested that shorter abutment height is associated with greater marginal bone loss in cemented prostheses, our in-silico study on prosthetic abutments with shorter collar heights showed better biomechanical behavior for all prosthetic components. and cortical bone, regardless of implant height. Shorter abutments allow selecting of abutments with larger diameters, increasing crown retention and improving crown-abutment-implant connection stability and accessibility during impression procedures [44, 54].

Furthermore, implants with higher I:P ratios positively affect peri-implant marginal bone level (MBL): within the P: I range of 0.6 - 2.36, higher I:P ratios correlate negatively with MBL peri-implant. [55] Clinically, these implants may still achieve good survival rates in the short and medium term, provided that the occlusion and parafunctional habits are controlled [52, 55, 58-60]. In addition, the placement of implants with an exchange of platforms and the use of long abutments connecting cement-retained crowns to the implants would provide greater height for restoration of biological width, allowing for easier removal of excess cement from soft tissues and would reduce inflammation induced by bacteria, thus preventing the progression of the lesion. Marginal bone loss in cemented restorations, but with a greater possibility of the set, due to the greater lever arm [51]. More studies are still needed to investigate the strength of the system, in turn providing a displacement map of the different structures. It is possible to fully characterize the potential strain of the implant-abutment system.

5. Conclusions

Based on the outcomes of this in vitro and silico study, the following conclusions may be drawn:

1. Long collar abutments negatively affect the biomechanical behavior of single structure supported by morse taper implants, and the greatest stresses are located in the prosthetic abutment;
2. The increase in the length of the abutment profile results in greater stress on the bone crest, thus hurting cortical bone stress values;
3. Cancellous bone tension showed no relationship with abutment-implant or abutment lengths.

Author Contributions: Conceptualization: J.D.M.d.M., I.J.S.J, D.A.Q., S.L.d.S., and G.d.R.S.L.; methodology, J.D.M.d.M., I.J.S.J, D.A.Q., S.L.d.S., and G.d.R.S.L.; formal analysis, J.D.M.d.M., I.J.S.J, M.A.C.S., D.A.Q., S.L.d.S., R.A.d.S., and G.d.R.S.L.; investigation, J.D.M.d.M., I.J.S.J, D.A.Q., S.L.d.S., R.A.d.S., N.C.R., and G.d.R.S.L; resources, J J.D.M.d.M., I.J.S.J., D.A.Q., S.L.d.S., R.A.d.S., A.B.B., N.C.R., and G.d.R.S.L.; data curation, J.D.M.d.M., D.A.Q., N.C.R., and A.L.S.B.; writing—J.D.M.d.M., I.J.S.J, M.A.C.S., D.A.Q., S.L.d.S., R.A.d.S., A.B.B., N.C.R., M.A.B., M.S.J., G.d.R.S.L., and A.L.S.B.; review and editing, J.D.M.d.M., D.A.Q., A.B.B., and G.d.R.S.L; supervision, M.A.C.S., M.S.J., M.A.B., G.R.d.S.L., and A.L.S.B.; project administration, M.A.C.S., M.A.B., M.S.J., G.R.d.S.L., and A.L.S.B.; funding acquisition, J.D.M.d.M. All authors have read and agreed to the published version of the manuscript.

Funding: This research was funded by the São Paulo Research Foundation (FAPESP – grant numbers 2019/24903-6, and 2021/11499-2).

Institutional Review Board Statement: Not applicable.

Informed Consent Statement: Not applicable.

Data Availability Statement: Data are available upon request.

Acknowledgments: The authors appreciate the support of Titaniumfix (®) (Titaniumfix, CNPJ: 468 01.786.547/0001-27, São José dos Campos, SP, Brazil); by donating the implants, abutments, screws, and STL files used 40 in this research.

Conflicts of Interest: The authors declare no conflicts of interest.

References

1. Quirynen, M.; Naert, I.; Van Steenberghe, D. Fixture design and overload influence marginal bone loss and fixture success in the Brånemark system. *Clin. Oral Implant. Res*. **1992**, 3, 104–111.
2. Mericske-Stern, R.; Venetz, E.; Fahrländer, F.; Bürgin, W. In vivo force measurements on maxillary implants supporting a fixed prosthesis or an overdenture: A pilot study. *J. Prosthet. Dent*. **2000**, 84, 535–547.
3. Isidor, F. Influence of forces on peri-implant bone. *Clin. Oral Implant. Res*. **2006**, 17, 8–18.

4. Cehreli, M.; Duyck, J.; De-Cooman, M.; Puers, R.; Naert, I. Implant design, and interface force transfer. A photoelastic and strain- gauge analysis. *Clin. Oral Implants. Res*. **2004**, 15, 249–257.
5. Tribst, J.P.M.; Dal Piva, A.M.O.; Bottino, M.A.; Nishioka, R.S.; Borges, A.L.S.; Özcan, M. Digital Image Correlation and Finite Element Analysis of Bone Strain Generated by Implant-Retained Cantilever Fixed Prosthesis. *Eur. J. Prosthodont. Restor. Dent*. **2020**, 28, 10–17.
6. Huang, H.L.; Huang, J.S.; Ko, C.C.; Hsu, J.T.; Chang, C.H.; Chen, M.Y. Effects of a splinted prosthesis supported a wide implant or two implants: A three-dimensional finite element analysis. *Clin. Oral Implant. Res*. **2005**, 16, 466–472.
7. Hollweg, H.; Jacques, L.B.; da Silva Moura, M.; Bianco, V.C.; Souza, E.A.; Rubo, J.H. Deformation of implant abutments after framework connection using strain gauges. *J. Oral Implantol*. **2012**, 38, 125–132.
8. Matos, J.D.; Arcila, L.V.; Ortiz, L.P.; Lopes, G.R.; Anami, L.C.; Ramos, N.C.; Saavedra, G.S.; Tribst, J.P.; Bottino, M.A. Hybrid abutment during prosthetic planning and oral rehabilitation. *Minerva Dent Oral Sci*. **2022**, 71(2), 107-116.
9. Suedam, V.; Souza, E.A.; Moura, M.S.; Jacques, L.B.; Rubo, J.H. Effect of abutment's height and framework alloy on the load distribution of mandibular cantilevered implant-supported prosthesis. *Clin. Oral Implant. Res*. **2009**, 20, 196–200.
10. Suedam, V.; Moretti-Neto, R.T.; Sousa, E.A.; Rubo, J.H. Effect of cantilever length and alloy framework on the stress distribution in the peri-implant area of cantilevered implant-supported fixed partial dentures. *J. Appl. Oral Sci*. **2016**, 24, 114–120.
11. Matos, J.D.M.d.; Lopes, G.d.R.S.; Queiroz, D.A.; Pereira, A.L.J.; Sinhoreti, M.A.C.; Ramos, N.d.C.; Lino, V.; de Oliveira, F.R.; Borges, A.L.S.; Bottino, M.A. Influence of the Peek Abutments on Mechanical Behavior of the Internal Connections Single Implant. *Materials* **2022**, 15, 8133.
12. Tribst, J.P.; Rodrigues, V.A.; Dal Piva, A.O.; Borges, A.L.; Nishioka, R.S. The importance of correct implant positioning and masticatory load direction on a fixed prosthesis. J. Clin. Exp. Dent. 2017, 10, e81–e87.
13. ISO 14801; International Organization for Standardization. Dentistry—Implants—Dynamic Fatigue Test for Endosseous Dental Implants, 3rd ed. International Organization for Standardization: Geneva, Switzerland, **2016**, 3, 9.
14. Lopes, G.d.R.S.; Matos, J.D.M.d.; Queiroz, D.A.; Tribst, J.P.M.; Ramos, N.d.C.; Rocha, M.G.; Barbosa, A.B.; Bottino, M.A.; Borges, A.L.S.; Nishioka, R.S. Influence of Abutment Design on Biomechanical Behavior to Support a Screw-Retained 3-Unit Fixed Partial Denture. *Materials* **2022**, 15, 6235.
15. Tribst, J.P.M.; Dal Piva, A.M.d.O.; Rodrigues, V.A.; Borges, A.L.S.; Nishioka, R. S. Stress and strain distributions on short implants with two different prosthetic connections–an in vitro and in silico analysis. *Braz Dent Scienc*. **2017**, 20, 101-109.
16. Matos, J.D.M.d.; Queiroz, D.A.; Nakano, L.J.N.; Andrade, V.C.; Ribeiro, N.d.C.R.; Borges, A.L.S.; Bottino, M.A.; Lopes, G.d.R.S. Bioengineering Tools Applied to Dentistry: Validation Methods for In Vitro and In Silico Analysis. *Dent. J*. **2022**, 10, 145.
17. Cicciù, M.; Bramanti, E.; Cecchetti, F.; Scappaticci, L.; Guglielmino, E.; Risitano, G. FEM and Von Mises analyses of different dental implant shapes for masticatory loading distribution. *Oral Implantol*. **2014**, 7, 1-10.
18. Osman, R.B.; Elkhadem, A.H.; Ma, S.; Swain, M.V. Titanium versus zirconia implants supporting maxillary overdentures: three-dimensional finite element analysis. *Int. J. Oral Maxillofac. Implants*. **2013** Sep-Oct, 28(5), e198-208.
19. Bottino, M.A.; de Oliveira, F.R.; Sabino, C.F.; Dinato, J.C.; Silva-Concílio, L.R.; Tribst, J.P.M. Survival Rate and Deformation of External Hexagon Implants with One-Piece Zirconia Crowns. *Metals (Basel)* **2021**, 11, 1068.
20. Souza, A.C.; Xavier, T.A.; Platt, J.A.; Borges, A.L. Effect of Base and Inlay Restorative Material on the Stress Distribution andFracture Resistance of Weakened Premolars. *Oper. Dent*. **2015**, 40, E158–E166.
21. Borges, A.L.S.; Costa, A.K.F.; Dal Piva, A.M. de O.; Pinto, A.B.A.; Tribst, J.P.M. Effect of Three Different Veneering Techniques on the Stress Distribution and in Vitro Fatigue Behavior of Core-Veneer All-Ceramic Fixed Partial Dentures. *J. Dent. Res. Dent. Clin. Dent. Prospects* **2021**, 15, 188–196.
22. Anami, L.C.; Lima, J.M.C.; Takahashi, F.E.; Neisser, M.P.; Noritomi, P.Y.; Bottino, M.A. Stress distribution around osseointegrated implants with different internal-cone connections: photoelastic and finite element analysis. *J Oral Implantol*. **2015**, 41, 155-62.
23. Tribst, J.P.M.; Dal Piva, A.M.O.; Özcan, M.; Borges, A.L.S.; Bottino, M.A. Influence of Ceramic Materials on Biomechanical Behavior of Implant Supported Fixed Prosthesis with Hybrid Abutment. *Eur J Prosthodont Restor Dent*. **2019**, 27, 76-82.
24. Valente, M.L.C.; Bolfarini, C.; Oliveira, D.P.; Dos Reis, A.C. Dental mini-implant designs to support overdentures: Development, biomechanical evaluation, and 3D digital image correlation. *J Prosthet Dent*. **2021**, 24, S0022-3913.
25. Tiossi, R.; Vasco, M.A.; Lin, L.; Conrad, H.J.; Bezzon, O.L.; Ribeiro, R.F.; Fok, A.S. Validation of finite element models for strainanalysis of implant-supported prostheses using digital image correlation. *Dent. Mater*. **2013**, 29, 788–796.
26. Tanasić, I.; Šarac, D.; Mitrović, N.; Tihaček-Šojić, L.; Mišković, Ž.; Milić-Lemić, A.; Milošević, M. Digital image correlation analysis of vertically loaded cylindrical Ti-implants with straight and angled abutments. *Exp Tech*. **2016**, 40, 1227-1233.
27. Frost, H.M. Wolff's Law and bone's structural adaptations to mechanical usage: an overview for clinicians. *Angle Orthod*. **1994**, 64, 175-88.
28. Terheyden, H.; Lang, N.P.; Bierbaum, S.; Stadlinger, B. Osseointegration - communication of cells. *Clin Oral Implants Res*. **2012**, 23, 1127-35.
29. Utiyama, K. A. U.; Menezes, F. C.; Catarina, M. V.; Sousa, D. R.; Silva, S. L. Determination of the mean relative photoelastic dispersion factor by means of photoelasticity. *Rev Bras Fis Tec Aplic*. **2022**, 9, 14-27.
30. Silva, S. L.; Jesus, M. A.; Silva, C. R.; Toffoli, D. J.; Camargo, U. N. Análise quantitativa de tensões em amostras fotoelásticas por meio de fotoelasticidade. *Rev Bras Fis Tec Aplic*. **2017**, 4, 34-51.

31. Shinya, A.; Ballo, A.M.; Lassila, L.V.; Shinya, A.; Närhi, T.O.; Vallittu, P.K. Stress and strain analysis of the bone-implant interface: a comparison of fiber-reinforced composite and titanium implants utilizing 3-dimensional finite element study. *J Oral Implantol*. **2011**, 37, 133-40.
32. Choi, A.H.; Matinlinna, J.P.; Ben-Nissan, B. Finite element stress analysis of Ti-6Al-4V and partially stabilized zirconia dental implant during clenching. *Acta Odontol Scand*. **2012**,70,353-61.
33. Gross, M.D.; Nissan, J.; Samuel, R. Stress distribution around maxillary implants in anatomic photoelastic models of varying geometry. Part I. *J Prosthet Dent*. **2001**, 85, 442-9.
34. Hasan, I.; Rahimi, A.; Keilig, L.; Brinkmann, K.T.; Bourauel, C. Computational simulation of internal bone remodeling around dental implants: a sensitivity analysis. *Comput Methods Biomech Biomed Engin*. **2012**,15,807-14.
35. Matos, J.D.M.; Dos Santos, A.C.M.; Nakano, L.J.N.; Vasconcelos, J.E.L.; Andrade, V.C.; Nishioka, R.S.; Bottino, M.A.; Lopes, G.R.S. Metal alloys in dentistry: an outdated material or required for oral rehabilitation? *Int. J. Odontostomat*. **2021**,15(3), 702-711.
36. Van Steenberghe D, Quirynen M, Naert I, Maffei G, Jacobs R. Marginal bone loss around implants retaining hinging mandibular overdentures, at 4-, 8- and 12-years follow-up. J Clin Periodontol. **2001**, 28, 628-33.
37. Närhi TO, Hevinga M, Voorsmit RA, Kalk W. Maxillary overdentures retained by splinted and unsplinted implants: a retrospective study. Int J Oral Maxillofac Implants **2001**,16,259-66.
38. González, J.E.G.; Mirza-Rosca, J.C. Study behavior of titanium and some of its alloys for biomedical and dental implant applications. *J Electroanal Chem*. **1999**, 471, 109–115.
39. Machado, L.S.; Bonfante, E.A.; Anchieta, R.B.; Yamaguchi, S.; Coelho, P.G. Implant-abutment connection designs for anterior crowns: reliability and failure modes. *Implant Dent*. **2013**,22,540-5.
40. Schmitt, C.M.; Nogueira-Filho, G.; Tenenbaum, H.C.; Lai, J.Y.; Brito, C.; Döring, H.; Nonhoff, J. Performance of conical abutment (Morse Taper) connection implants: a systematic review. *J Biomed Mater Res A*. **2014**, 102, 552-74.
41. Quaranta, A.; Piemontese, M.; Rappelli, G.; Sammartino, G.; Procaccini, M. Technical and biological complications related to crown to implant ratio: a systematic review. *Implant Dent*. **2014**,23,180-7.
42. Kourtis, S.; Damanaki, M.; Kaitatzidou, S.; Kaitatzidou, A.; Roussou, V. Loosening of the fixing screw in single implant crowns: predisposing factors, prevention and treatment options. *J Esthet Restor Dent*. **2017**,29,233-246.
43. Sakamoto, K.; Homma, S.; Takanashi, T.; Takemoto, S.; Furuya, Y.; Yoshinari, M.; Yajima, Y. Influence of eccentric cyclic loading on implant components: Comparison between external joint system and internal joint system. *Dent Mater J*. **2016**, 35, 929-937.
44. Gracis, S.; Thompson, V.P.; Ferencz, J.L.; Silva, N.R.; Bonfante, E.A. A new classification system for all-ceramic and ceramic-like restorative materials. *Int J Prosthodont*. **2015**, 28, 227-35.
45. Naert, I.; Duyck, J.; Vandamme, K. Occlusal overload and bone/implant loss. *Clin Oral Implants Res*. **2012**, 23, 95-107.
46. Rieger, M.R.; Mayberry, M.; Brose, M.O. Finite element analysis of six endosseous implants. *J Prosthet Dent*. **1990**,63,671-6.
47. Ortega-Oller, I.; Suárez, F.; Galindo-Moreno, P.; Torrecillas-Martínez, L.; Monje, A.; Catena, A.; Wang, H.L. The influence of implant diameter on its survival: a meta-analysis based on prospective clinical trials. *J Periodontol*. **2014**, 85, 569-80.
48. Anitua, E.; Tapia, R.; Luzuriaga, F.; Orive, G. Influence of implant length, diameter, and geometry on stress distribution: a finite element analysis. *Int J Periodontics Restorative Dent*. **2010**, 30, 89-95.
49. Papavasiliou, G.; Kamposiora, P.; Bayne, S.C.; Felton, D.A. Three-dimensional finite element analysis of stress distribution around single tooth implants as a function of bony support, prosthesis type, and loading during function. *J Prosthet Dent*. **1996**, 76, 633-40.
50. Kozlovsky, A.; Tal, H.; Laufer, B.Z.; Leshem, R.; Rohrer, M.D.; Weinreb, M.; Artzi, Z. Impact of implant overloading on the peri-implant bone in inflamed and non-inflamed peri-implant mucosa. *Clin Oral Implants Res*. **2007**,18,601-10.
51. Spinato, S.; Galindo-Moreno, P.; Bernardello, F.; Zaffe, D. Minimum Abutment Height to Eliminate Bone Loss: Influence of Implant Neck Design and Platform Switching. *Int J Oral Maxillofac Implants*. **2018**, 33, 405–411.
52. Galindo-Moreno, P.; León-Cano, A.; Monje, A.; Ortega-Oller, I.; O'Valle, F.; Catena, A. Abutment height influences the effect of platform switching on peri-implant marginal bone loss. *Clin Oral Implants Res*. **2016**, 27, 167-73.
53. Siadat, H.; Pirmoazen. S.; Beyabanaki, E.; Alikhasi, M. Does Abutment Collar Length Affect Abutment Screw Loosening After Cyclic Loading? *J Oral Implanto*l. **2015**, 41 Spec No:346-51.
54. Garaicoa-Pazmiño, C.; Del Amo, F.S.L.; Monje, A.; Catena, A.; Ortega-Oller, I.; Galindo-Moreno, P.; Wang, H.L. Influence of crown/implant ratio on marginal bone loss: a systematic review. *J Periodontol*. **2014** , 85(9):1214-21.
55. Tribst, J.P.M.; Morais, D.C.; Matos, J.D.M.d.; Lopes, G.d.R.S.; Dal Piva, A.M.O.; Borges, A.L.S.; Bottino, M.A.; Lanzotti, A.; Martorelli, M.; Ausiello, P. Influence of Framework Material and Posterior Implant Angulation in Full-Arch All-on-4 Implant-Supported Prosthesis Stress Concentration. *Dent J (Basel)*. **2022**, 14;10, 1-12.
56. Vasconcelos, J.E.L.; Matos, J.D.M.; Queiroz, D.A.; Lopes, G.D.R.S.; Lacerda, B.C.G.V.; Bottino, M.A.; Turssi, C.P.; Basting, R.T.; Amaral, F.L.B.; França, F.M.G. Implant-Abutment Misfit after Cyclic Loading: An In Vitro Experimental Study. *Materials (Basel)*. **2022**, 15(15), 5341.
57. Tribst, J.P.M.; Dal Piva, A.M.O.; Borges, A.L.S.; Bottino, M.A. Influence of the crown and hybrid abutment ceramic materials on the stress distribution of implant-supported prosthesis. *Rev Odontol UNESP*. **2018**, 47, 149-154.
58. Bidez, M.W.; Misch, C.E. Force transfer in implant dentistry: basic concepts and principles. *J Oral Implantol*. **1992**,18,264-274.

59. Matos, J.D.M.; Lopes, G.D.R.S.; Nakano, L.J.N.; Ramos, N.C.; Vasconcelos, J.E.L.; Bottino, M.A.; Tribst, J.P.M. Biomechanical evaluation of 3-unit fixed partial dentures on monotype and two-piece zirconia dental implants. *Comput Methods Biomech Biomed Engin*. **2022**, 25(3), 239-246.
60. Bidez, M.W.; Misch, C.E. Issues in bone mechanics related to oral implants. *Implant Dent*. **1992**,1,289-294.